

A Global Comparison of Ekman Pumping From Satellite Scatterometers and Ocean Data Assimilation Estimates

Paulo S. Polito
Tong Lee and Ichiro Fukumori

INPE - National Institute for Space Research, Brazil
Jet Propulsion Laboratory/Caltech, USA

Motivation

Ekman pumping, a form of wind-driven upwelling, plays important roles in upper-ocean dynamics, thermodynamics, and biology as well as in boundary-layer meteorology.

Inverse models, such as those of ECCO (Estimation of the Circulation and Climate of the Ocean, <http://www.ecco-group.org/>), estimate wind forcing through ocean data assimilation.

Ekman pumping obtained from scatterometer is compared with those derived from ECCO models which assimilate TOPEX/POSEIDON (T/P) derived sea level anomalies using the adjoint and Kalman filter/smoothing methods.

Differences in Ekman pumping are quantified and changes due to the assimilation are analyzed to identify the spectral area over which it has a significant impact.

The comparison also highlights aspects where the ECCO model and assimilation schemes need improvement.

Objectives

The objectives of this study are to:

1. Analyze the difference between the Ekman pumping estimates from different model designs:
 - (a) forward (simulation),
 - (b) adjoint (assimilation)
 - (c) Kalman filter/smoothing,
2. Compare the sea surface height anomaly from T/P with that obtained from the models.
3. For each model/data comparison analyze the difference in several areas of the period-wavelength spectrum associated to known dynamical phenomena.
4. Suggest possible model improvements based on the analysis above.

Introduction

The Ekman pumping w_e is an estimate of wind-driven vertical velocity, directly related to the curl of the wind stress:

$$w_e = \frac{\nabla \times \vec{\tau}}{\rho f}$$

This is a first order estimate that works within the constraints of the Ekman theory.

The wind stress is estimated from satellite scatterometer wind vectors, accurate to approximately 1ms^{-1} and 20° .

Estimates of sea surface height anomaly from the T/P altimeter are assimilated by the adjoint and Kalman filter/smoothing methods.

In turn, the models yield the Ekman pumping fields that would be necessary to create the assimilated sea surface height anomaly.

These Ekman pumping fields are compared to the scatterometer measurements. This comparison is performed within several areas of the zonal-temporal spectrum.

Data and Methods

The altimeter-derived sea surface height anomaly η was obtained from the WOCE TOPEX/POSEIDON data distributed by JPL/PODAAC.

The interpolated η_o is decomposed through a series of zonal-temporal finite impulse response (2D FIR) filters [2, 3] in the following components (numeric subscripts indicate the \sim period in months):

$$\eta_o = \underbrace{\eta_t}_{\text{Basin}} + \underbrace{\eta_{24} + \eta_{12} + \eta_6 + \eta_3}_{\text{Rossby waves}} + \underbrace{\eta_1}_{\text{TIWs}} + \underbrace{\eta_{K6} + \eta_{K3} + \eta_{K1}}_{\text{Kelvin waves}} + \underbrace{\eta_E + \eta_r}_{\text{eddies}}$$

From ERS-1/2 scatterometer winds the stress τ is calculated via LKB method [1] using SST fields from the Reynolds dataset [4] and water vapor estimates from SSM/I.

Through the analysis of the η components we obtain the filter parameters (phase speed and wavelength) used to decompose the Ekman pumping (w_e) fields.

This way both the Ekman pumping and the sea surface height components refer to the same spectral area, associated with specific dynamical regimes.

"Simulation" refers to the model run without T/P data assimilation, "Assimilation" refers to the model run with T/P data assimilation, and "Kalman" refers to the Kalman filter/smoothing model.

Description of the Models

Adjoint

The model referred to as Model-X uses the X method and assumes that Y. The Model-X run in this study uses the following set-up: a, b, c, etc. As a consequence we expect Model-X to reproduce the following aspects of the ocean physics.

Forward

The model referred to as Model-X uses the X method and assumes that Y. The Model-X run in this study uses the following set-up: a, b, c, etc. As a consequence we expect Model-X to reproduce the following aspects of the ocean physics.

Kalman

The model referred to as Model-X uses the X method and assumes that Y. The Model-X run in this study uses the following set-up: a, b, c, etc. As a consequence we expect Model-X to reproduce the following aspects of the ocean physics.

Results

Pacific 2.5°N - Comparison of η and w_e

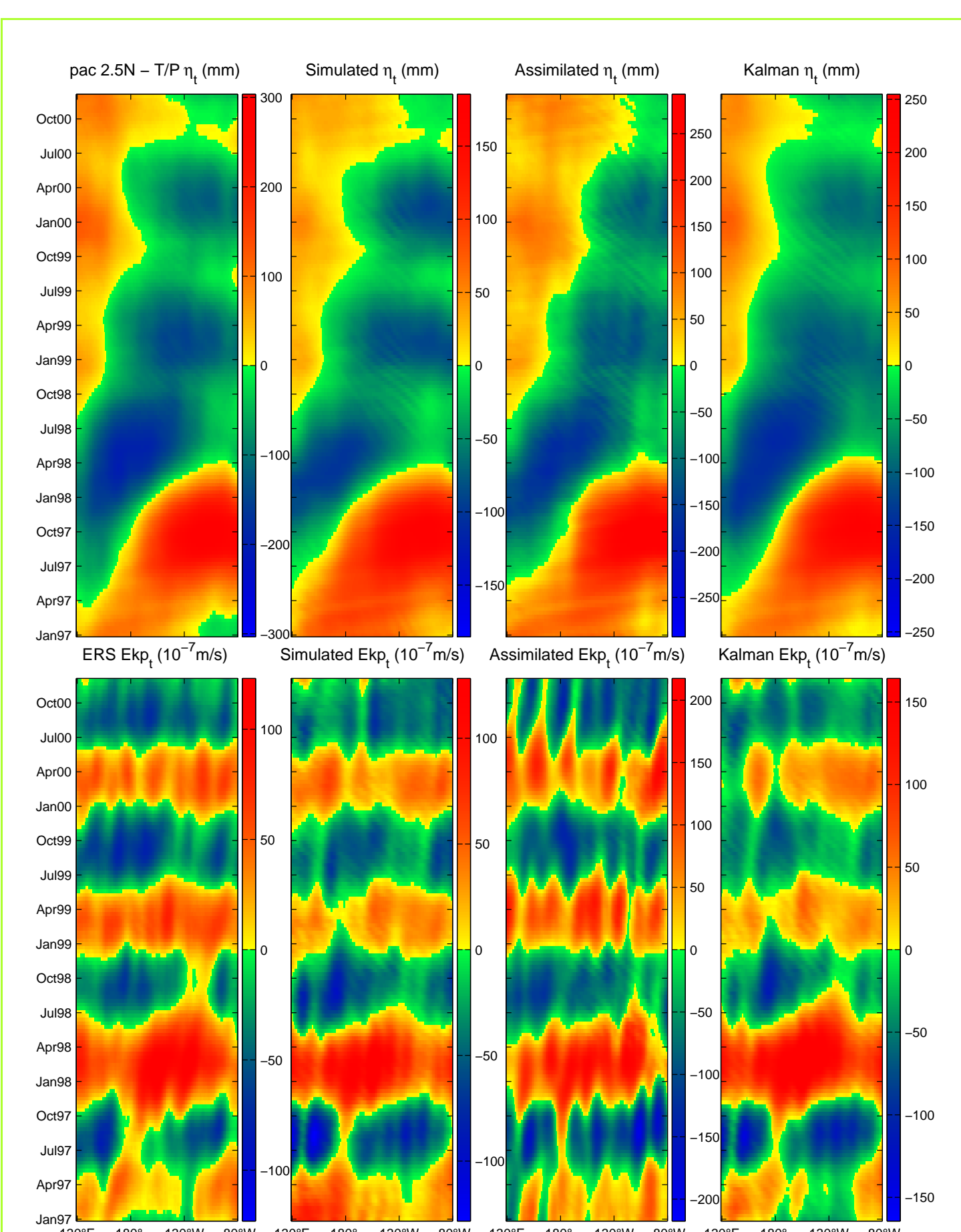


Figure 1: Zonal-temporal (Hovmöller) diagrams for the basin-scale, non-propagating components (η_t , $w_{e,t}$) for the Pacific at 2.5°N . The top row shows sea-surface height anomalies (in mm) and the bottom row shows Ekman pumping (in m/s). The left column shows the FIR filtered satellite data, the middle column shows the simulated model data, and the right column shows the assimilated model data.

Pac 2.5°N	$R_{\eta,s}$	$R_{\eta,a}$	$R_{\eta,k}$	$R_{w,s}$	$R_{w,a}$	$R_{w,k}$
	0.44	0.23	0.23	0.53	1.13	0.68
	$\sigma_{\eta,s}$	$\sigma_{\eta,a}$	$\sigma_{\eta,k}$	$\sigma_{w,s}$	$\sigma_{w,a}$	$\sigma_{w,k}$
	0.80	0.95	0.95	0.72	-0.28	0.54
	$C_{\eta,s}$	$C_{\eta,a}$	$C_{\eta,k}$	$C_{w,s}$	$C_{w,a}$	$C_{w,k}$
	0.96	0.97	0.98	0.87	0.80	0.87

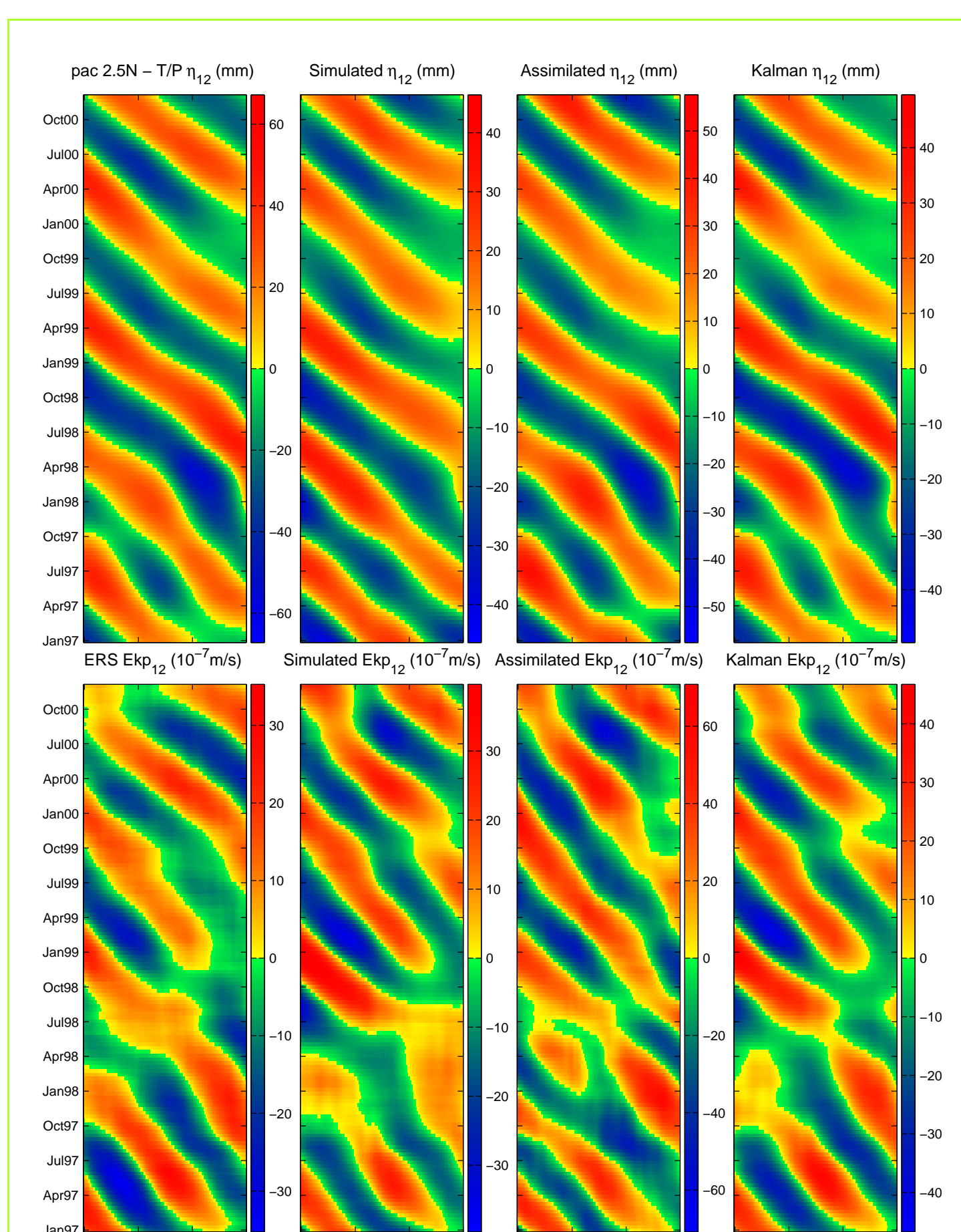


Figure 2: Similar to Figure 1 for the components (η_{12} , $w_{e,12}$) associated to annual Rossby waves.

Pac 2.5°N	$R_{\eta,s}$	$R_{\eta,a}$	$R_{\eta,k}$	$R_{w,s}$	$R_{w,a}$	$R_{w,k}$
	0.51	0.35	0.35	0.72	1.48	0.64
	$\sigma_{\eta,s}$	$\sigma_{\eta,a}$	$\sigma_{\eta,k}$	$\sigma_{w,s}$	$\sigma_{w,a}$	$\sigma_{w,k}$
	0.74	0.88	0.87	0.48	-1.19	0.59
	$C_{\eta,s}$	$C_{\eta,a}$	$C_{\eta,k}$	$C_{w,s}$	$C_{w,a}$	$C_{w,k}$
	0.88	0.94	0.96	0.77	0.71	0.88

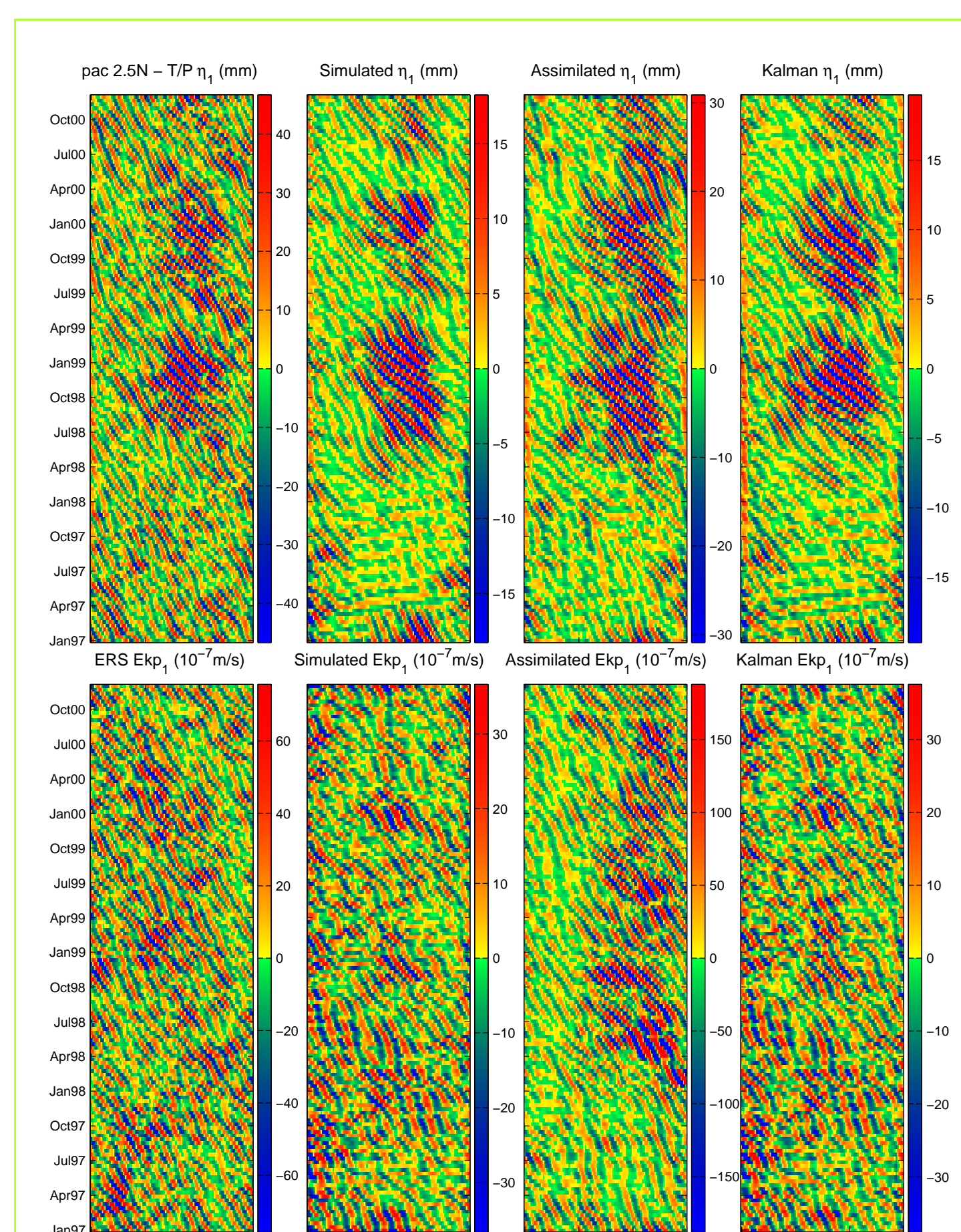


Figure 3: Similar to Figure 1 for the components (η_1 , $w_{e,1}$) associated to tropical instability waves.

Pac 2.5°N	$R_{\eta,s}$	$R_{\eta,a}$	$R_{\eta,k}$	$R_{w,s}$	$R_{w,a}$	$R_{w,k}$
	1.11	1.02	1.07	1.12	2.66	1.09
	$\sigma_{\eta,s}$	$\sigma_{\eta,a}$	$\sigma_{\eta,k}$	$\sigma_{w,s}$	$\sigma_{w,a}$	$\sigma_{w,k}$
	-0.22	-0.03	-0.14	-0.25	-6.06	-0.18
	$C_{\eta,s}$	$C_{\eta,a}$	$C_{\eta,k}$	$C_{w,s}$	$C_{w,a}$	$C_{w,k}$
	-0.09	0.31	0.04	-0.02	0.02	0.06

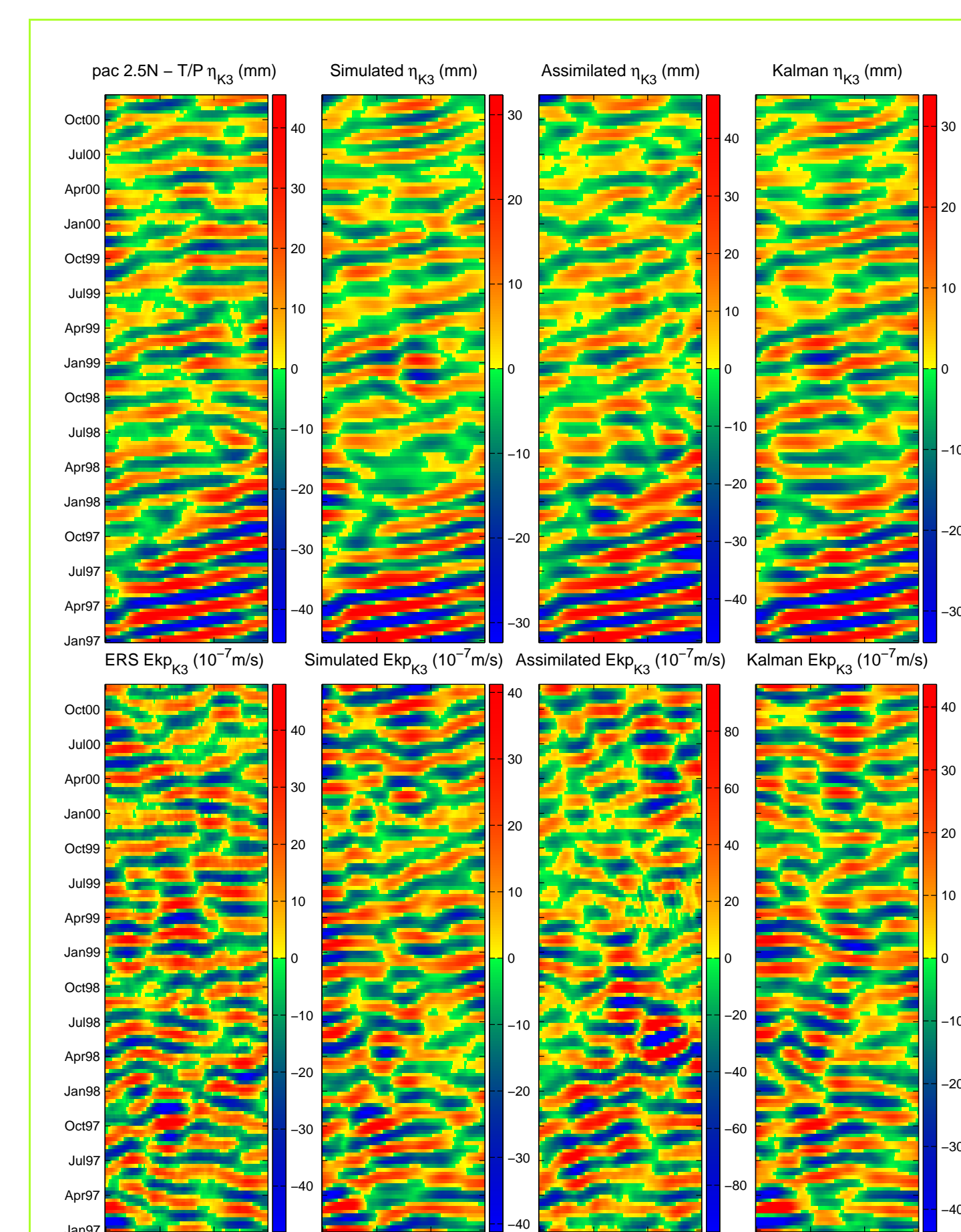


Figure 4: Similar to Figure 1 for the components (η_{K3} , $w_{e,K3}$) associated to Kelvin waves with 2-3 months period.

Pac 2.5°N	$R_{\eta,s}$	$R_{\eta,a}$	$R_{\eta,k}$	$R_{w,s}$	$R_{w,a}$	$R_{w,k}$
	0.93	0.82	0.57	1.06	2.06	0.98
	$\sigma_{\eta,s}$	$\sigma_{\eta,a}$	$\sigma_{\eta,k}$	$\sigma_{w,s}$	$\sigma_{w,a}$	$\sigma_{w,k}$
	0.13	0.33	0.67	-0.12	-3.25	0.04
	$C_{\eta,s}$	$C_{\eta,a}$	$C_{\eta,k}$	$C_{w,s}$	$C_{w,a}$	$C_{w,k}$
	0.45	0.68	0.82	0.36	0.19	0.48

Results

Pacific 10.5°N - Comparison of η and w_e

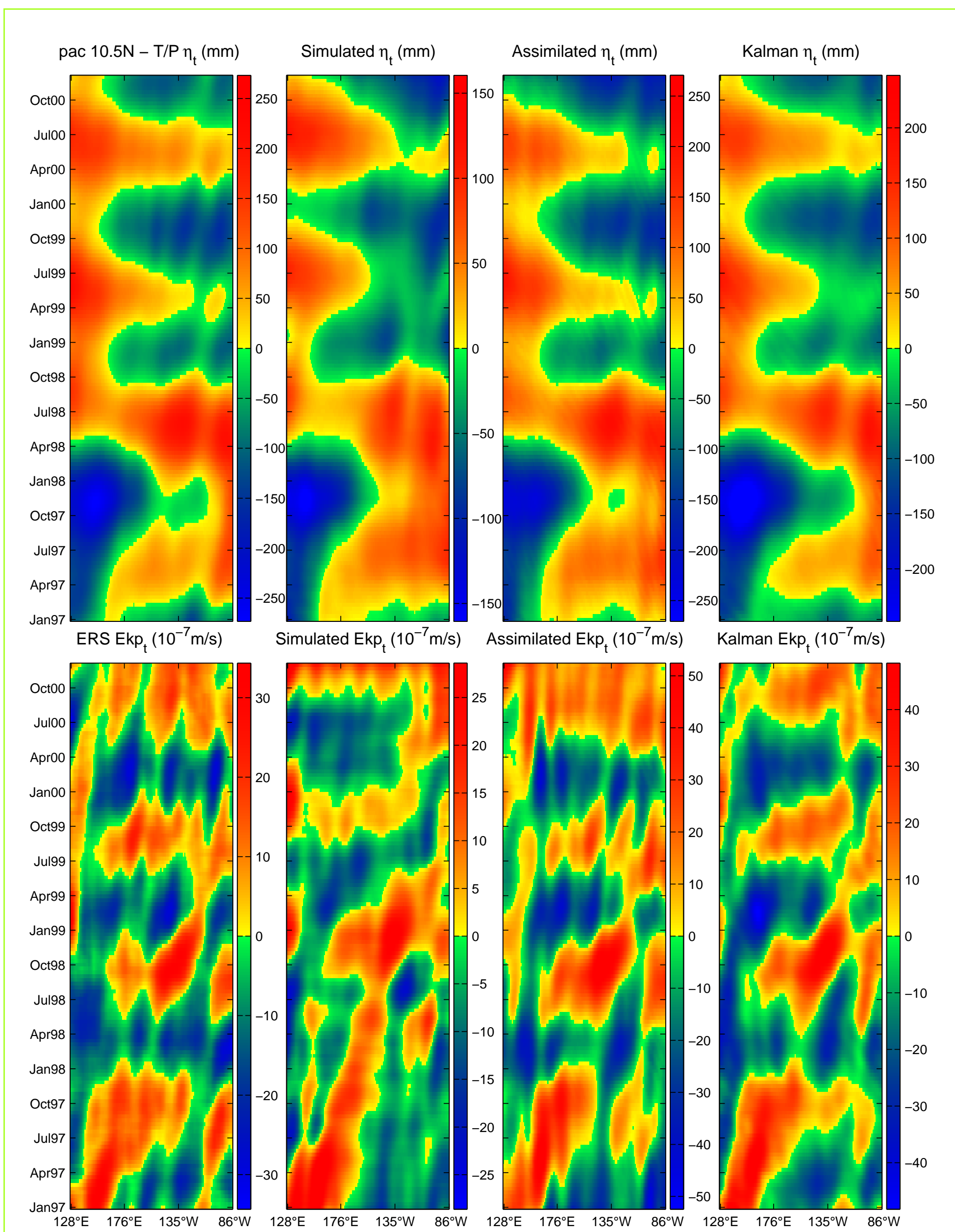


Figure 5: Similar to Figure 1 for 10.5°N.

Pac 10.5°N	$R_{\eta,s}$	$R_{\eta,a}$	$R_{\eta,k}$	$R_{w,s}$	$R_{w,a}$	$R_{w,k}$
	0.55	0.33	0.27	1.01	1.08	0.89
	$\sigma_{\eta,s}$	$\sigma_{\eta,a}$	$\sigma_{\eta,k}$	$\sigma_{w,s}$	$\sigma_{w,a}$	$\sigma_{w,k}$
	0.70	0.89	0.92	0.02	-0.17	0.21
	$C_{\eta,s}$	$C_{\eta,a}$	$C_{\eta,k}$	$C_{w,s}$	$C_{w,a}$	$C_{w,k}$
	0.89	0.95	0.96	0.36	0.19	0.48

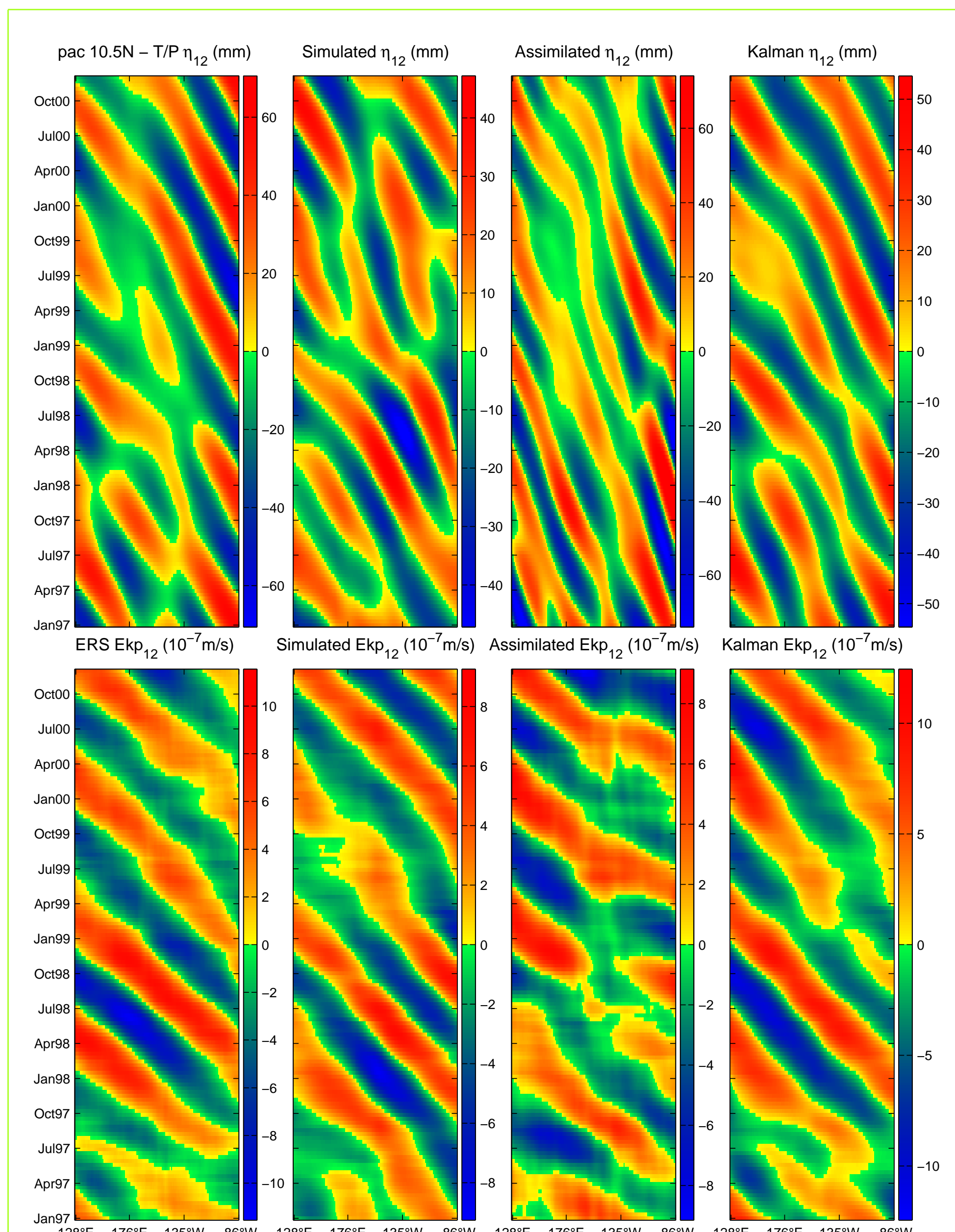


Figure 6: Similar to Figure 5 for η_{12} and w_{e12} , annual Rossby waves.

Pac 10.5°N	$R_{\eta,s}$	$R_{\eta,a}$	$R_{\eta,k}$	$R_{w,s}$	$R_{w,a}$	$R_{w,k}$
	1.12	0.80	0.64	1.02	0.85	0.81
	$\sigma_{\eta,s}$	$\sigma_{\eta,a}$	$\sigma_{\eta,k}$	$\sigma_{w,s}$	$\sigma_{w,a}$	$\sigma_{w,k}$
	-0.26	0.37	0.59	-0.03	0.28	0.34
	$C_{\eta,s}$	$C_{\eta,a}$	$C_{\eta,k}$	$C_{w,s}$	$C_{w,a}$	$C_{w,k}$
	0.14	0.70	0.77	0.38	0.57	0.69

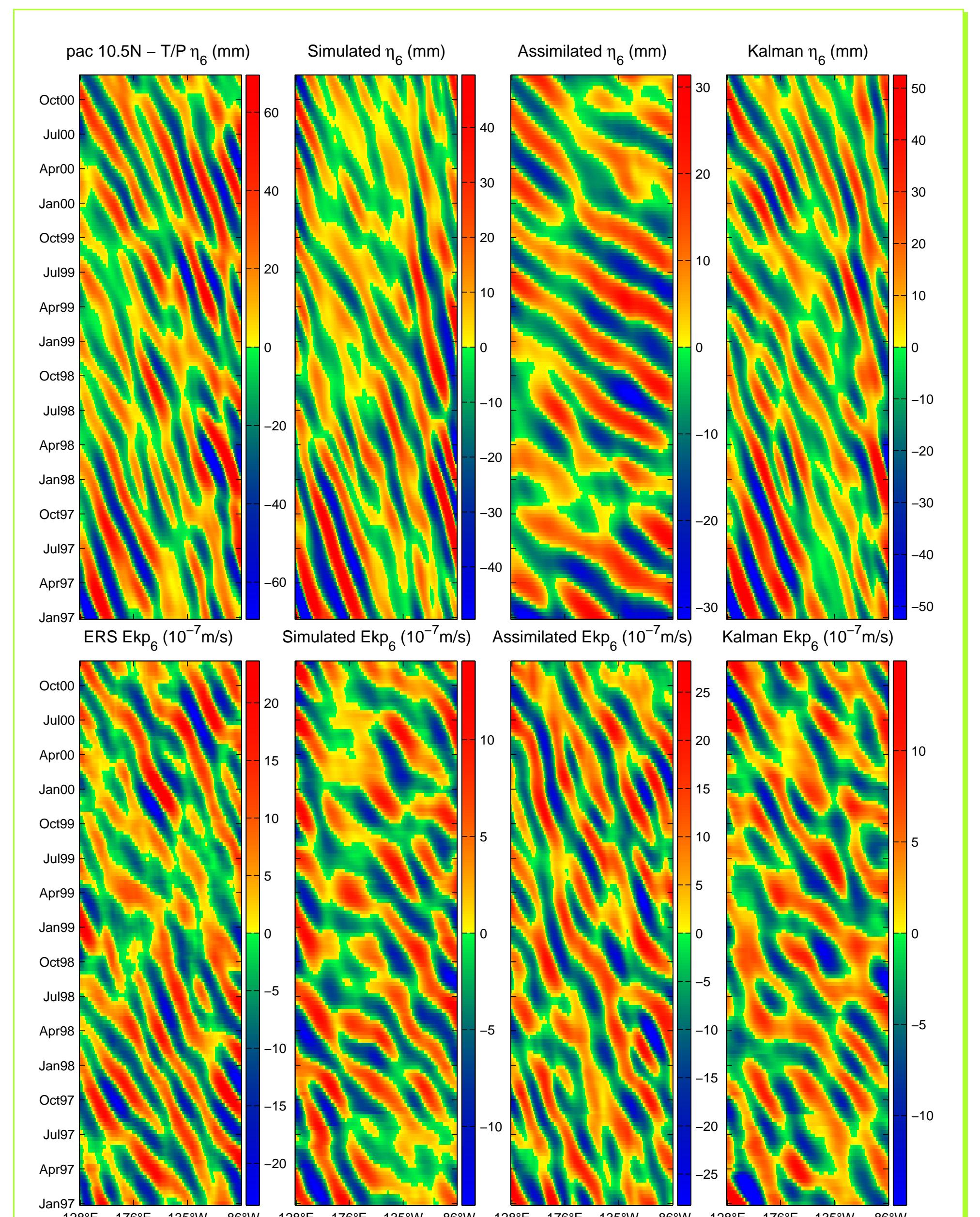


Figure 7: Similar to Figure 5 for η_6 and w_{e6} , semi-annual Rossby waves.

Pac 10.5°N	$R_{\eta,s}$	$R_{\eta,a}$	$R_{\eta,k}$	$R_{w,s}$	$R_{w,a}$	$R_{w,k}$
	1.01	0.96	0.64	1.06	1.41	1.08
	$\sigma_{\eta,s}$	$\sigma_{\eta,a}$	$\sigma_{\eta,k}$	$\sigma_{w,s}$	$\sigma_{w,a}$	$\sigma_{w,k}$
	-0.03	0.07	0.59	-0.13	-0.98	-0.16
	$C_{\eta,s}$	$C_{\eta,a}$	$C_{\eta,k}$	$C_{w,s}$	$C_{w,a}$	$C_{w,k}$
	0.34	0.31	0.77	0.19	0.19	0.19

Atlantic 27.5°N - Comparison of η and w_e

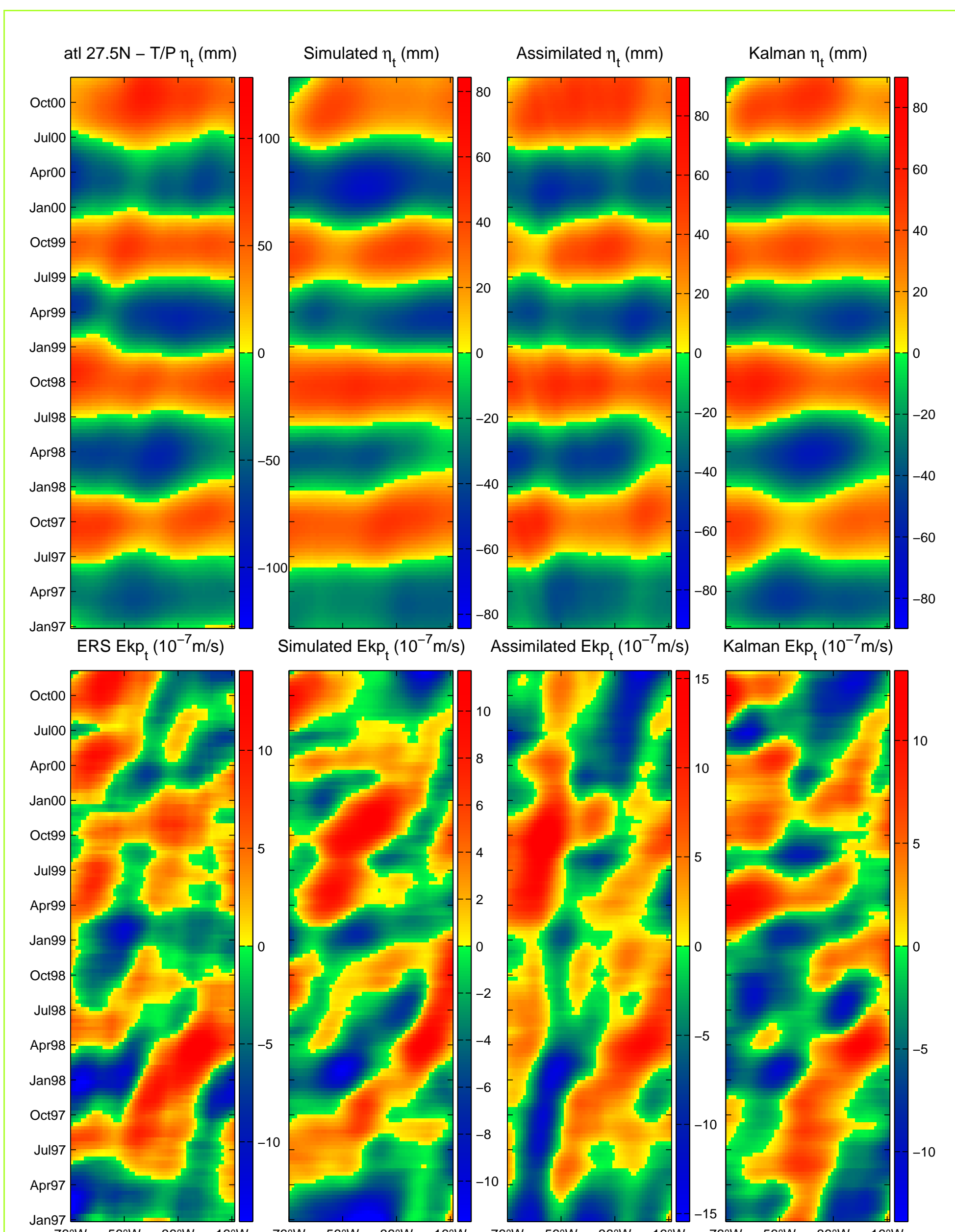


Figure 8: Similar to Figure 1 for 27.5°N in the Atlantic.

Atl 27.5°N	$R_{\eta,s}$	$R_{\eta,a}$	$R_{\eta,k}$	$R_{w,s}$	$R_{w,a}$	$R_{w,k}$
	0.53	0.40	0.39	0.90	1.07	0.95
	$\sigma_{\eta,s}$	$\sigma_{\eta,a}$	$\sigma_{\eta,k}$	$\sigma_{w,s}$	$\sigma_{w,a}$	$\sigma_{w,k}$
	0.72	0.84	0.85	0.19	-0.13	0.10
	$C_{\eta,s}$	$C_{\eta,a}$	$C_{\eta,k}$	$C_{w,s}$	$C_{w,a}$	$C_{w,k}$
	0.88	0.94	0.95	0.53	0.49	0.53

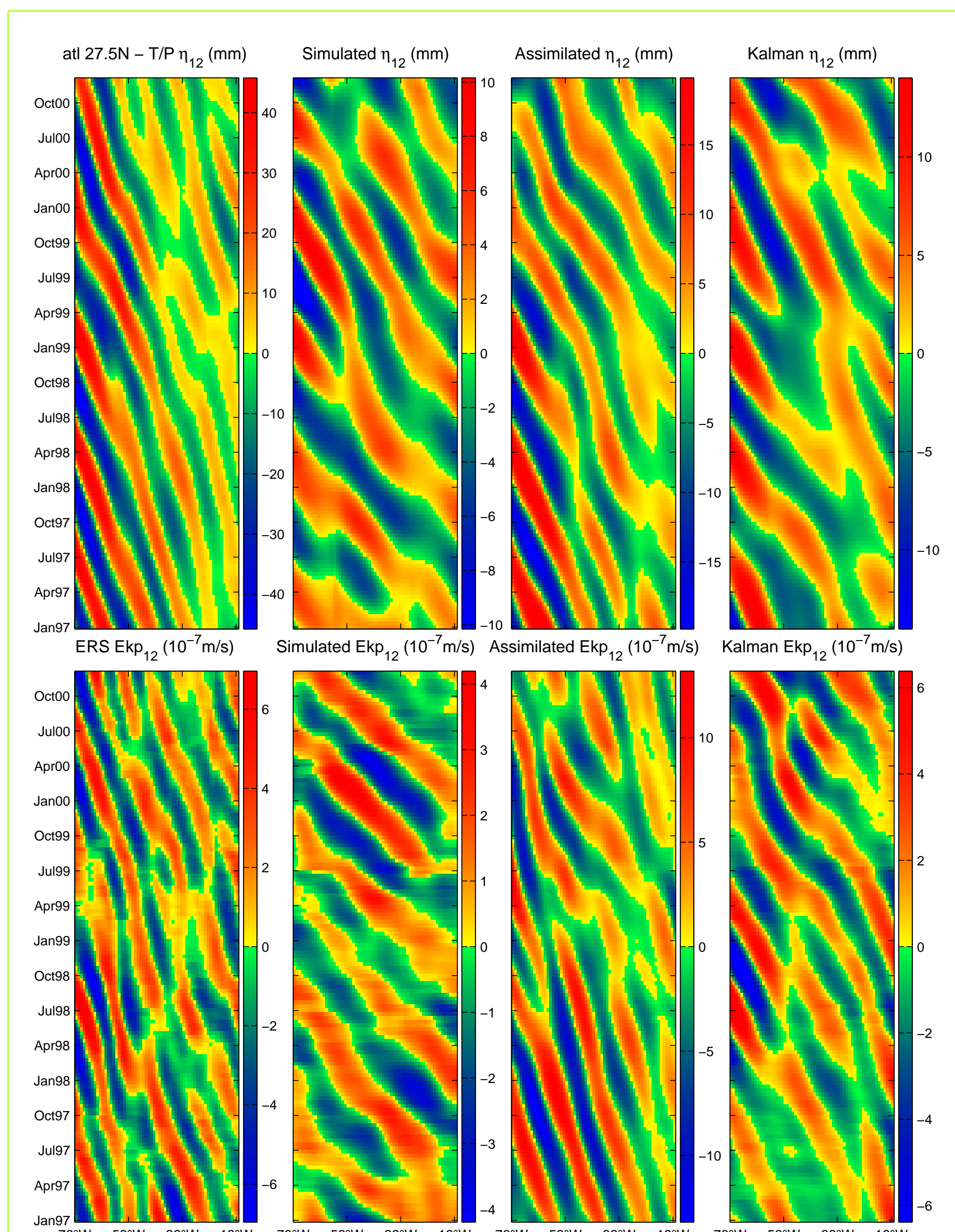


Figure 9: Similar to Figure 8 for η_{12} and w_{e12} , annual Rossby waves.

Atl 27.5°N	$R_{\eta,s}$	$R_{\eta,a}$	$R_{\eta,k}$	$R_{w,s}$	$R_{w,a}$	$R_{w,k}$
	0.93	0.72	0.88	1.09	1.93	1.16
	$\sigma_{\eta,s}$	$\sigma_{\eta,a}$	$\sigma_{\eta,k}$	$\sigma_{w,s}$	$\sigma_{w,a}$	$\sigma_{w,k}$
	0.13	0.48	0.22	-0.19	-2.73	-0.35
	$C_{\eta,s}$	$C_{\eta,a}$	$C_{\eta,k}$	$C_{w,s}$	$C_{w,a}$	$C_{w,k}$
	0.40	0.77	0.52	0.14	0.23	0.27

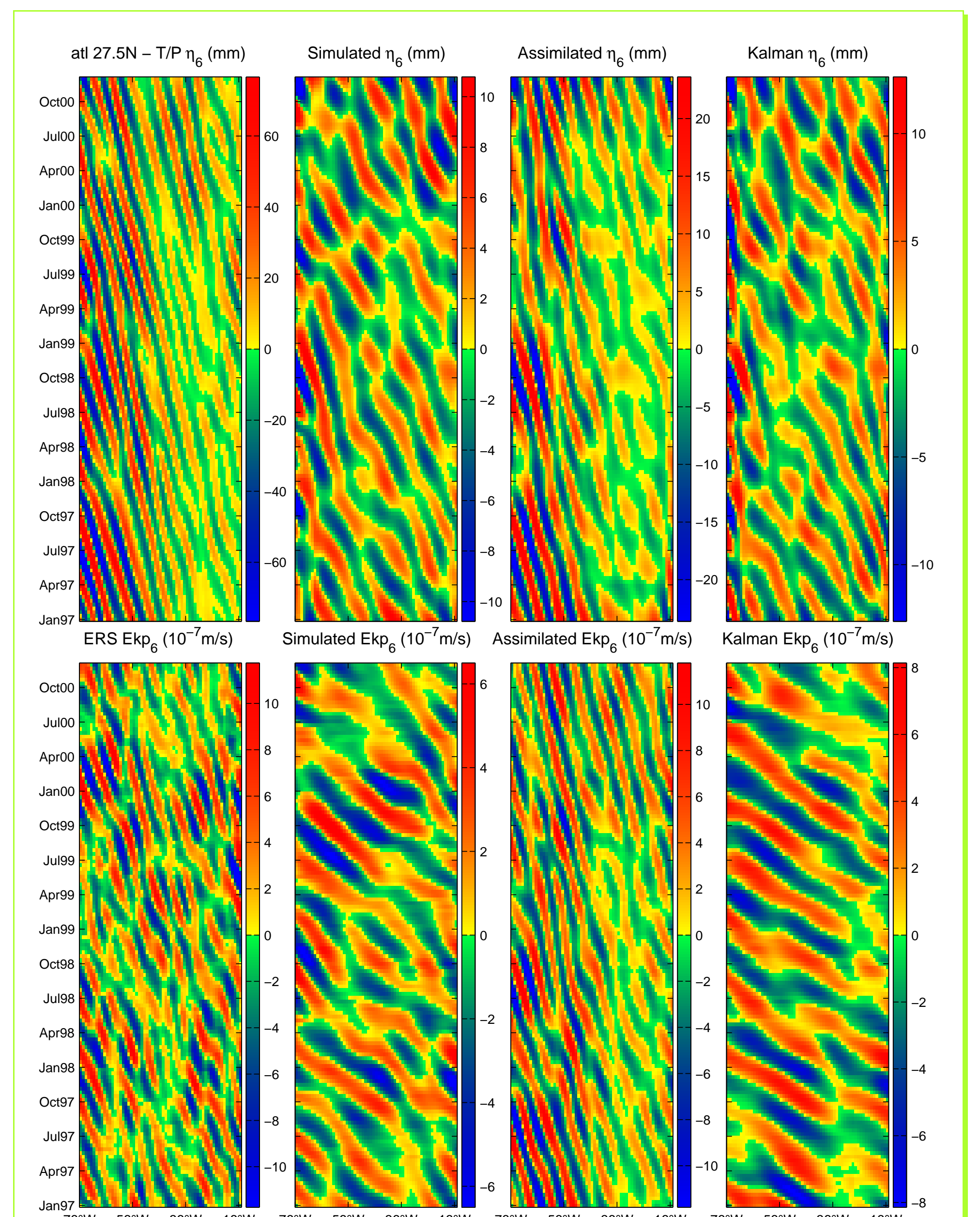


Figure 10: Similar to Figure 8 for η_6 and w_{e6} , semi-annual Rossby waves.

Atl 27.5°N	$R_{\eta,s}$	$R_{\eta,a}$	$R_{\eta,k}$	$R_{w,s}$	$R_{w,a}$	$R_{w,k}$
	1.00	0.84	1.00	1.11	1.35	1.16
	$\sigma_{\eta,s}$	$\sigma_{\eta,a}$	$\sigma_{\eta,k}$	$\sigma_{w,s}$	$\sigma_{w,a}$	$\sigma_{w,k}$
	0.00	0.29	0.00	-0.23	-0.81	-0.34
	$C_{\eta,s}$	$C_{\eta,a}$	$C_{\eta,k}$	$C_{w,s}$	$C_{w,a}$	$C_{w,k}$
	0.07	0.63	0.09	0.07	0.10	0.10

Concluding Remarks

For sea surface height anomalies (η) the assimilation and Kalman filter/smoothing runs improve on the simulation results. In all tested cases except one it reduces the rms difference ($R_{\eta,a} < R_{\eta,s}$), increases the fractional variance ($\sigma_{\eta,a} > \sigma_{\eta,s}$) and the correlation between data and model ($C_{\eta,a} > C_{\eta,s}$).

For the Ekman pumping estimates (w_e) only the Kalman filter/smoothing assimilation improves the statistics at 2.5°N and 10.5°N for most components. At 27.5°N none of the assimilation schemes gave positive results.

In most figures the Ekman pumping patterns from data assimilation models are qualitatively more similar to the satellite derived patterns than the simulation runs.

Results are relatively better for the low-frequency, large

wavelength end of the spectrum. As a consequence, results are generally better at low latitudes.

Apparently, the models reproduce better the Pacific basin than the Atlantic or Indian (not shown).

References

- [1] W. T. Liu, K. B. Katsaros, and J. A. Businger. Bulk parameterizations of air-sea exchanges of heat and water vapor including the molecular constraints at the interface. *Journal of Atmospheric Sciences*, 36:1722–1735, 1979.

- [2] P. S. Polito, O. T. Sato, and W. T. Liu. Characterization and validation of heat storage variability from Topex/Poseidon at four oceanographic sites. *Journal of Geophysical Research*, 105(C7):16,911–16,921, 2000.
- [3] P. S. Polito, O. T. Sato, and W. T. Liu. Global characterization of Rossby waves at several spectral bands. In print. *Journal of Geophysical Research*, 2002.
- [4] R. W. Reynolds and T. M. Smith. Improved global sea surface temperature analyses using optimum interpolation. *Journal of Climate*, 7:929–948, 1994.

Contact: For more details, please e-mail us: Paulo S. Polito (polito@ltd.inpe.br)

Acknowledgments: P. S. Polito was fully supported by the Fundação para Amparo à Pesquisa do Estado de São Paulo (FAPESP) under project 01-06921-3.